

Galaxy Clusters with Chandra¹

W. Forman¹, C. Jones¹, M. Markevitch^{1,3}, A. Vikhlinin^{1,3}, & E. Churazov^{2,3}

1) Smithsonian Astrophysical Observatory, Cambridge, MA, USA

2) MPI fur Astrophysik, Garching, Germany

3) Space Research Institute, Moscow, Russia

Abstract We discuss Chandra results related to 1) cluster mergers and cold fronts and 2) interactions between relativistic plasma and hot cluster atmospheres. We describe the properties of cold fronts using NGC1404 in the Fornax cluster and A3667 as examples. We discuss multiple surface brightness discontinuities in the cooling flow cluster ZW3146. We review the supersonic merger underway in CL0657. Finally, we summarize the interaction between plasma bubbles produced by AGN and hot gas using M87 and NGC507 as examples.

0.1 Cluster Formation at High Angular Resolution

For many years clusters were thought to be dynamically relaxed systems evolving slowly after an initial, short-lived episode of violent relaxation. However, while the dynamical timescale for the richest cluster cores is comfortably less than the Hubble time, other less dense clusters have dynamical timescales comparable to or longer than the age of the Universe [21]. X-ray images, starting with Einstein and continuing with ROSAT and ASCA, and now with Chandra and XMM-Newton, provide a powerful technique to “map” the structure in the gravitational potential of massive systems containing hot gaseous atmospheres.

The X-ray observations supported the now prevalent idea that structure in the Universe has grown through gravitational amplification of small scale instabilities or hierarchical clustering. At one extreme, some clusters grow, in their final phase, through mergers of nearly equal mass components. Such mergers can be spectacular events involving kinetic energies as large as $\sim 10^{64}$ ergs, the most energetic events since the Big Bang. More common are smaller mergers and accretion of material from large scale filaments. The ROSAT image of A85 shows the relationship between large scale structure and cluster merging where small groups are detected infalling along a filament into the

¹Contribution to XIII Rencontres de Blois 2001, ed. L. M. Celnikier

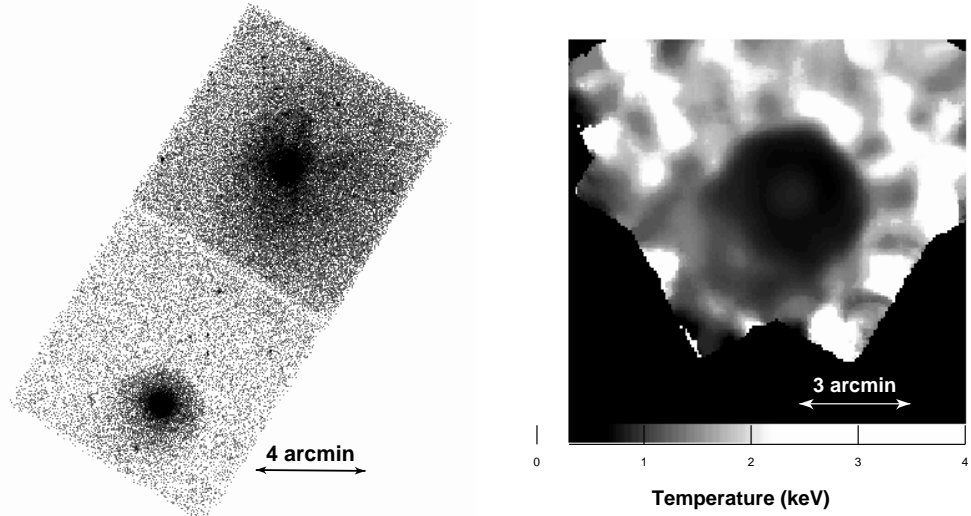


Figure 1: The ACIS observation of NGC1404 and NGC1399. (a) shows the 0.5–2.0 keV band image of the Fornax cluster. The gas filled dark halo surrounding NGC1404 is at the lower left (southeast) while the cluster core, dominated by the halo surrounding NGC1399 lies at the upper right (northwest). (b) The temperature map of the Fornax region. The cold core surrounding NGC1404 has a temperature of less ~ 1 keV while the surrounding gas has a temperature of 1.5 keV.

main cluster [10]. Chandra and XMM with high angular resolution and high throughput provide new insights into cluster formation and evolution.

Cluster Cold Fronts Prior to the launch of Chandra, sharp gas density discontinuities had been observed in the ROSAT images of A2142 and A3667 [26]. Since both clusters exhibited characteristics of major mergers, these features were expected to be shock fronts. However, the first Chandra observations showed that these were not shocks, but a new kind of structure – cold fronts [25]. Their study has provided new and detailed insights into the physics of the intracluster medium (ICM) [37, 38].

Fig. 1a shows a striking example of a cold front as NGC1404 and its gaseous corona approaches the cluster center (to the northwest) [9]. The image clearly shows the sharp edge of the surface brightness discontinuity, shaped by the ram pressure of the cluster gas. The temperature map (Fig. 1b) confirms that the infalling cloud is cold compared to the hotter Fornax ICM.

Physics of Cold Fronts The best studied cold front is that in A3667 ($z = 0.055$). Although expected to exhibit a shock front based on its ROSAT image [26], the sharp feature observed in the Chandra observation is the boundary of a dense cold cloud, a merger remnant [37, 38]. The surface brightness profile, converted to gas density, and the gas temperature distribution yield the gas pressure on both sides of the cold front. The difference between the two pressures is a measure of the ram pressure of the ICM on the moving cold front. Hence, the precise measurement of the gas parameters yields

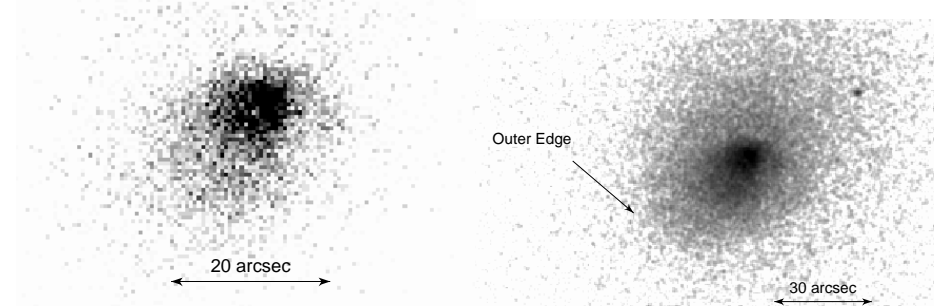


Figure 2: Multiple X-ray surface brightness edges in ZW3146 ($z = 0.296$). (a) The 0.5-2.0 keV image of the central region of ZW3146 shows the two inner edges at $3''$ and $8''$. (b) The right panel shows the edge at $35''$.

the cloud velocity. The factor of two difference in pressures between the free streaming region and the region immediately inside the cold front yields a Mach number of the cloud of 1 ± 0.2 ($1430 \pm 290 \text{ km s}^{-1}$) [37].

In addition to the edge, a weak shock is detected. The distance between the cold front and the weak shock ($\sim 350 \text{ kpc}$) and the observed gas density jump at the shock (a factor of 1.1-1.2) yield the shock’s propagation velocity, $\sim 1600 \text{ km s}^{-1}$, which is consistent with that derived independently from the pressure jump across the cold front [37].

The A3667 observation provides important information on the efficiency of transport processes in clusters. As the surface brightness profile shows (see [37]), the density “edge” is very sharp. Quantitatively, Vikhlinin et al. found that the width of the front was less than $3.5''$ (5 kpc). This sharp edge requires that transport processes across the edge be suppressed, presumably by magnetic fields. Without such suppression, the edge should be broader since the electron Coulomb mean free path is about 13 kpc, several times the width of the cold front [37]. Furthermore, Vikhlinin et al. observed that the cold front appears sharp only over a sector of about $\pm 30^\circ$ centered on the direction of motion, while at larger angles, the sharp boundary disappears [38]. The disappearance can be explained by the onset of Kelvin-Helmholtz instabilities, as the ambient ICM gas flows past the moving cold front. To explain the observed extent of the sharp boundary, the instability must be partially suppressed, e.g., by a magnetic field parallel to the boundary with a strength of $7 - 16 \mu\text{G}$ with a corresponding pressure of only 10-20% of the thermal pressure [38].

ZW3146 – Multiple “Fronts” ZW3146 is a moderately distant ($z = 0.2906$; $5.74 \text{ kpc per arcsec}$) cluster with a remarkably high mass deposition rate that was estimated to exceed $1000 \text{ M}_\odot \text{ yr}^{-1}$ [11]. The Chandra image further demonstrates the remarkable nature of this cluster – on scales from $3''$ to $30''$ ($\sim 20 \text{ kpc}$ to 170 kpc), three separate X-ray surface brightness edges are detected (see Fig. 2 and Forman et al. [16]). At the smallest radii, two edges are seen to the northwest and north of the center (see Fig. 2a). The first, at a radius of $\sim 3''$ (17 kpc), spans an angle of nearly 180° with a surface brightness drop of almost a factor of 2. The second edge, at a radius of $\sim 8''$ (45 kpc) spans only 90° but has a surface brightness drop of almost a factor of 4. The third edge

(see Fig. 2b) lies to the southeast, about $35''$ (200 kpc) from the cluster center, has a decrease of about a factor of 2, and, as with the first edge, extends over an angle of almost 180° .

The variety of morphologies and scales exhibited by these sharp edges or cold fronts is quite remarkable. Possibly the edges may arise from moving cold gas clouds that are the remnants of merger activity as observed in A2142 and A3667 or as oscillations (or “sloshing”) of the cool gas at the center of the cluster potential as observed in A1795 [27]. The extremely regular morphology of ZW3146 on large linear scales seems to exclude a recent merger and, hence, “sloshing” of the gas seems the more likely explanation for the observed edges. High resolution, large scale structure simulations show that dense halos, formed at very early epochs, survive cluster collapse [19, 20]. While most of the dark matter halos, having galaxy size masses, are associated with the sites of galaxy formation, the larger mass halos also may survive (without their gas) or may have fallen into the cluster only recently. Hence, we might expect to find a range of halo mass distributions moving within the cluster potential. We speculate that, as these halos move, the varying gravitational potential could accelerate the cool dense gas that has accumulated in the cluster core and could produce the “sloshing” needed to give rise to the multiple surface brightness edges observed in some clusters.

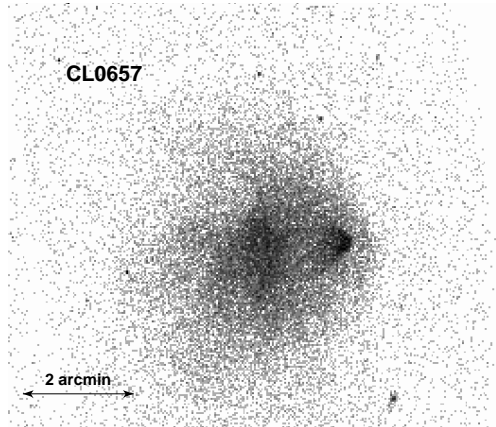


Figure 3: The Chandra image of the cluster CL0657. The cluster exhibits the classic properties of a supersonic merger – a dense (cold) “bullet” traversing the hot cluster with a leading shock front (Mach cone). The gas parameters across the front imply the cold core is traversing the cluster at a supersonic velocity with a Mach number of $M \sim 2 - 3$. The disrupted core of the cluster can be seen to the east of the “bullet”.

CL0657 – A Prototypical Cluster Shock Front CL0657 ($z = 0.296$) was discovered by Tucker et al. as part of a search for “failed” clusters, clusters that were X-ray bright but had few, if any, optical galaxies [35]. From ASCA observations, this cluster was found to have a remarkably hot gas temperature of about 17 keV, making it the hottest cluster known [36].

The Chandra image of CL0657 shows the classic properties of a supersonic merger (see Markevitch et al. for a detailed discussion of this cluster [28]). We see a dense

(cold) core moving to the west after having traversed, and disrupted, the core of the main cluster. Leading the cold, dense core is a density discontinuity which appears as a shock front (Mach cone). The spectral data show that the gas to the east (trailing the shock) has been heated by the passage of the shock. The detailed gas density parameters confirm that the “bullet” is moving to the west with a velocity of $3000\text{--}4000\text{ km sec}^{-1}$, approximately 2-3 times the sound speed of the ambient gas. CL0657 is the first clear example of a relatively strong shock arising from cluster mergers.

0.2 The Radio—X-ray Connection – or Bubbles, Bubbles Everywhere

Prior to the launch of Chandra, ROSAT observations of NGC1275 and M87 provided hints of complex interactions between radio emitting plasmas ejected from AGN within the nuclei of dominant, central cluster galaxies [2, 3, 6, 7]. With the launch of Chandra, the interaction between relativistic plasma, with and without detected radio emission, and the hot intracluster medium (ICM) has been observed in many systems and is now a major area of investigation [12, 31, 13, 14, 39, 30, 23, 33, 32].

M87 and the Evolution of Buoyant Plasma Bubbles The 327 MHz high resolution, high dynamic range radio map (see Fig. 4) of M87 shows a well-defined torus-like eastern bubble and a less well-defined western bubble, both of which are connected to the central emission by a column, and two very faint almost circular emission regions northeast and southwest of the center [34]. The correlation between X-ray and radio emitting features has been remarked by several authors [15, 3, 22].

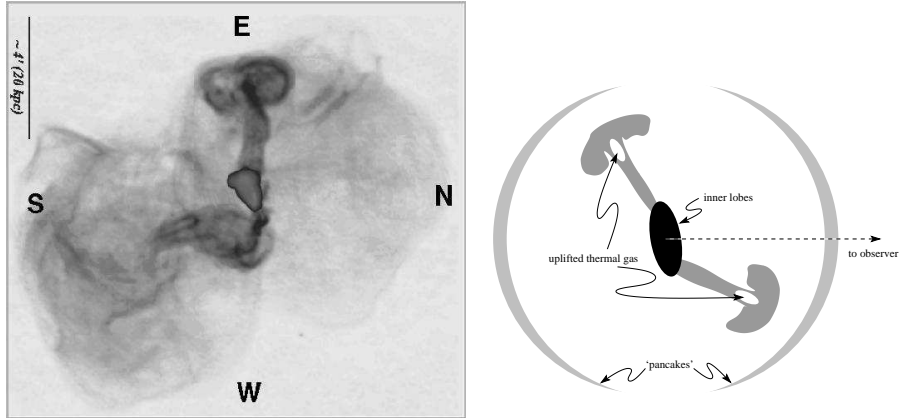


Figure 4: **Left:** $14'.6 \times 16'.0$ radio map of M87 (North to the right, East is up) (from Owen et al. [34]). **Right:** Suggested source geometry. The central black region denotes the inner radio lobes, the gray “mushrooms” correspond to buoyant bubbles already transformed into tori, and the gray lens-shaped structures are “pancakes” (seen edge-on) possibly formed by older bubbles [7].

Motivated by the similarity in appearance between M87 and hot bubbles rising in

a gaseous atmosphere, Churazov et al. developed a simple model of the M87 bubbles which is generally applicable to the many bubble-like systems seen in the Chandra observations [7]. Fig. 5 shows an initially buoyant bubble transform into a torus as it rises through a galaxy or cluster atmosphere.

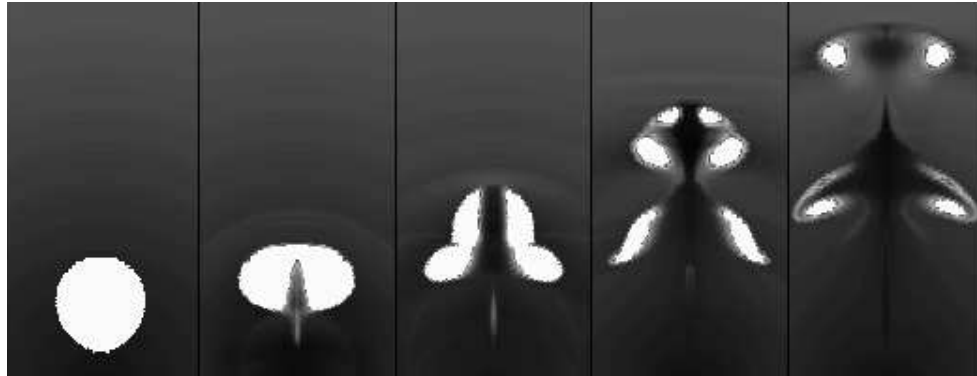


Figure 5: The gas temperature distribution at 0, 8.4, 21, 42, and 67 Myr. Each box is 40×20 kpc. The temperature is coded in the 0.7 (black) to 5 keV (white) range. The hot “radio-emitting plasma,” which initially has a temperature on the order of 100 keV, is white. The coldest gas is not at the center of the cooling flow but is associated with the rising bubble and is produced from uplifted, adiabatically expanded gas.

By entraining cool gas as it rises, the bubble produces a characteristic “mushroom” appearance, similar to an atmospheric nuclear explosion. This qualitatively explains the correlation of the radio and X-ray emitting plasmas and naturally accounts for the thermal nature of the X-ray emission associated with the rising torus [3, 4, 1]. Finally, in the last evolutionary phase, the bubble reaches a height at which the ambient gas density equals that of the bubble. The bubble then expands to form a thin layer (a “pancake”). The large low surface brightness features in the M87 radio map could be just such pancakes. In the simulations performed by Churazov et al. the buoyant bubbles behaved as expected and did produce the features observed in both X-rays and radio for M87. Although the exact form of the rising bubbles was sensitive to initial conditions, the toroidal structures were a common feature. Ambient gas was uplifted in the cluster atmosphere reducing the effects of cooling flows and producing the “stem” of the mushroom that is brighter than the surrounding regions [7]. Note that the XMM-Newton observation shows that the bright X-ray columns are cool, exactly as expected in the buoyant bubble scenario [1]. A sketch of the overall source structure of M87, based on the evolution of buoyant bubbles, is shown in Fig. 4 [7].

NGC507 - the central galaxy in a group NGC507 is the central galaxy in a nearby ($z = 0.016$) group that has been studied extensively in X-rays [24, 29, 5, 18]. The galaxy is the site of a weak B2 radio source (luminosity $\sim 10^{37}$ ergs s^{-1}) [8]. The Chandra X-ray image, shown in Fig. 6a, covers only the central, high surface brightness emission of the group around NGC507. The 0.5-2.0 keV surface brightness distribution shows sharp edges to the southwest, southeast and north, reminiscent of those in the clusters A2142 and A3667. In addition to the edges, there are two X-ray peaks. The first, to

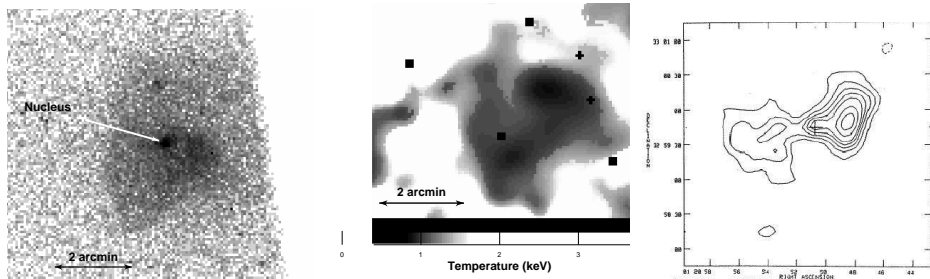


Figure 6: (a) The 0.5-2.0 keV surface brightness distribution of NGC507. (b) The temperature map of the central region of NGC507. The galaxy center is cool as are the regions to the west, the north-south edge to the east, and the edge to the south running from northwest to southeast. (c) The VLA radio map showing the central point source, a jet emanating to the west and two radio lobes [8]. The depression in the X-ray surface brightness to the west of the galaxy peak coincides with the western radio lobe.

the east, coincides with the nucleus of NGC507. A second peak, $1'$ to the west has no optical counterpart. However, comparing the X-ray and the radio map (Fig. 6a, c) shows that the western radio lobe lies precisely in the surface brightness trough between the nucleus and the peak to the west. Thus, it seems likely that the radio lobe, probably a buoyant bubble, has displaced X-ray emitting gas generating a trough in the X-ray surface brightness distribution.

The origin of the peculiar sharp surface brightness discontinuities around NGC507 is unclear. The bright emission is well fit by a thermal model with gas temperatures near 1 keV, consistent with the mean ASCA temperature of 1.10 ± 0.05 keV [29]. Detailed spectroscopic analyses were complicated by unexpected high background at high energies. A second Chandra observation is planned to allow detailed spectroscopy. The emission from the central region is resolved and hence the contribution from a central AGN is relatively small (see Forman et al. [16] for additional discussion of NGC507). Perhaps the X-ray surface brightness features arise either from motion of NGC507 and its dark halo within the larger group potential as suggested for the multiple edges in clusters [27].

0.3 Conclusions

We did not expect the rich variety of new structures seen in the Chandra high angular resolution observations of clusters and early type galaxies. Instead of confirming our prejudices, Chandra has brought us a wealth of new information on the interaction of radio sources with the hot gas in both galaxy and cluster atmospheres. We see “edges” in many systems with hot and cold gas in close proximity and have been able to extract important new parameters of the ICM. We have only barely begun to digest the import of the Chandra cluster and galaxy observations. We can only expect the unexpected as Chandra observations continue and as our understanding of how best to use this new observatory matures.

We acknowledge support from NASA contract NAS8 39073, NASA grants NAG5-3065 and NAG5-6749 and the Smithsonian Institution.

Note Added on ZW3146

One of the puzzles relating to the X-ray observation of ZW3146 was the apparent misalignment by a few arcseconds between the X-ray brightness peak and the optical center of the central, dominant cD galaxy. The solution to this apparent misalignment was resolved by the FIRST radio image which shows two radio sources with flux densities of ~ 2 mJy separated by $14''$ (see Fig. 7a). As Fig. 7b shows, the northern component of the pair of radio sources is precisely aligned with the optical cD galaxy at the cluster center. Fig. 7c shows that the radio source, and therefore the center of the cD galaxy, lies at the approximate center of irregular X-ray features. The bright X-ray structure northwest of the cD is elongated perpendicular to the direction to the galaxy center. A second X-ray bright feature lies southeast of the radio peak. We suggest that the radio emitting plasma formed a bubble that produced a trough in the X-ray surface brightness at the galaxy center. The bubble is surrounded by an irregular shell of X-ray emission. Thus, the brightest X-ray structures do not lie at the galaxy center, but instead form a partial shell surrounding the radio emitting plasma [17]. Such structures are similar to the X-ray surface brightness enhancements seen around radio plasma bubbles in nearby galaxies e.g., M84 [14].

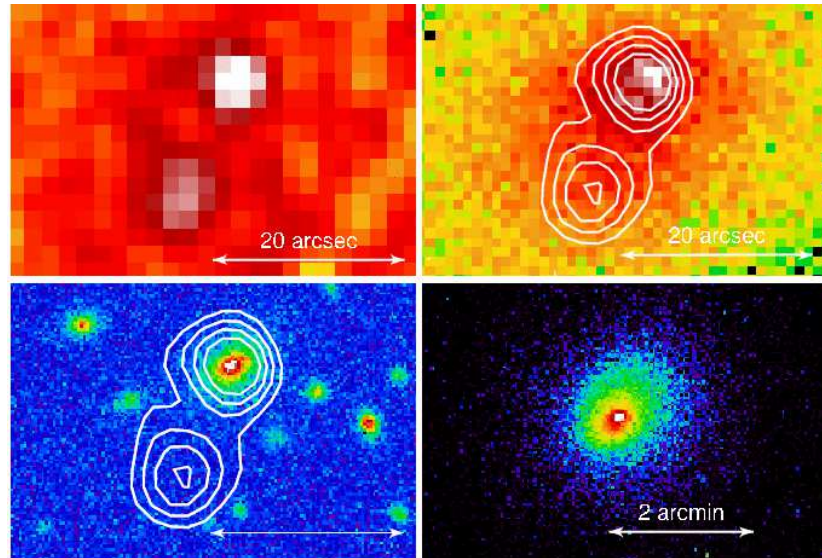


Figure 7: **(a - upper left)** The FIRST radio image of ZW3146 shows two radio sources with integrated fluxes of ~ 2 mJy. **(b - lower left)** Contours of the FIRST radio image superposed on an optical image (S. Allen and A. Edge, private communication) shows that the northern radio source is nearly perfectly aligned on the center of the optical cD galaxy at the cluster center. The second radio source may be a background object, unrelated to the cluster. **(c - upper right)** Contours from the FIRST radio image superposed on the Chandra full resolution ($0.492''$ pixel) image show that the radio emission is centered within an irregular shell of X-ray emission. **(d - lower right)** Large scale X-ray image of ZW3146.

Bibliography

- [1] Belsole et al.: A&A, **365**, L188 (2001)
- [2] H. Bohringer et al.: MNRAS **264**, L25 (1993)
- [3] H. Bohringer, P. Nulsen, R. Braun, A. Fabian: MNRAS **274**, L67 (1995)
- [4] Bohringer et al.: A&A, **365**, L181 (2001)
- [5] D. Buote & A. Fabian: MNRAS, **296**, 977 (1998)
- [6] E. Churazov, W. Forman, C. Jones, H. Bohringer: A&A, **356**, 788 (2000)
- [7] E. Churazov et al.: ApJ **554**, 261 (2001)
- [8] H. R. de Ruiter, P. Parma, P., C. Fanti, R. Fanti: A&AS, **65**, 111 (1986)
- [9] A. Dosaj, C. Jones, W. Forman, M. Markevitch, A. Vikhlinin: AAS Meeting Phoenix, **43.17**, (2002)
- [10] F. Durret, F. et al.: A&A, **335**, 41 (1998)
- [11] A. Edge et al.: MNRAS, **270**, L1 (1994)
- [12] A. Fabian et al.: MNRAS **318**, L65 (2000)
- [13] A. C. Fabian, A. Celotti, K.M. Blundell, N.E. Kassim, R.A. Perley: MNRAS in press, astro-ph/0111418 (2001)
- [14] A. Finoguenov, C. Jones: ApJL **547**, L107 (2001)
- [15] E. Feigelson, P. Wood, E. Schreier, D. Harris, M. Reid: ApJ **312**, 101 (1987)
- [16] W. Forman, M. Markevitch, C. Jones, A. Vikhlinin, E. Churazov, astro-ph/0110087 (2001)
- [17] W. Forman et al.: ApJ (2002)
- [18] Y. Fukazawa: PASJ, **50**, 187 (1998)
- [19] S. Ghigna, B. Moore, F. Governato, G. Lake, T. Quinn, J. Stadel: MNRAS, **300**, 146 (1998)

- [20] S. Ghigna, B. Moore, F. Governato, G. Lake, T. Quinn, J. Stadel: *ApJ*, **544**, 616 (2000)
- [21] J. Gunn, & R. Gott: *ApJ* **176**, 1 (1972)
- [22] D. Harris, F. N. Owen, J. A. Biretta, W. Junor: Diffuse Thermal and Relativistic Plasma in Galaxy Clusters eds. H. Böhringer, L. Feretti, P. Schuecker, MPE Report **271**, 111 (1999)
- [23] C. Jones et al. *ApJL* in press, astro-ph/0108114 (2001)
- [24] D. Kim & G. Fabbiano: *ApJ* **441**, 182 (1995)
- [25] M. Markevitch et al.: *ApJ* **541**, 542 (2000)
- [26] M. Markevitch, C. Sarazin, A. Vikhlinin: *ApJ* **521**, 526 (1999)
- [27] M. Markevitch, A. Vikhlinin, P. Mazzotta: *ApJL* **562**, L153 (2001)
- [28] M. Markevitch et al.: *ApJL* in press, astro-ph/0110468 (2001)
- [29] H. Matsumoto et al.: *ApJ* **482**, 133 (1997)
- [30] P. Mazzotta et al.: *ApJL* in press, astro-ph/0107557 (2001)
- [31] B. McNamara et al.: *ApJL* **534**, 135 (2000)
- [32] B. McNamara et al.: *ApJ* in press, astro-ph/0110554 (2001)
- [33] P. Nulsen et al. *ApJ* in press, astro-ph/0110523 (2001)
- [34] F. Owen, J. Eilek, N. Kassim: *ApJ* **543**, 611 (2000)
- [35] W. Tucker, H. Tananbaum, & R. Remillard: *ApJ* **444**, 532 (1995)
- [36] W. Tucker et al.: *ApJ* **496**, L5 (1998)
- [37] A. Vikhlinin, M. Markevitch, S. Murray: *ApJ* **551** 160 (2000a)
- [38] A. Vikhlinin, M. Markevitch, S. Murray: *ApJ* **549**, L47 (2000b)
- [39] J. Vrtilek et al. , in preparation and IAP 2000 Workshop (2001)